Probing Conformational Changes upon Photolysis: FTIR Studies of the Low Temperature Liganded and Photoproduct States of Oxy- and Carbonmonoxymyoglobin†

Lisa M. Miller and Mark R. Chance*

Contribution from the Department of Physiology and Biophysics, Albert Einstein College of Medicine of Yeshiva University, Bronx, New York 10461

Received May 3, 1994®

Abstract: Fourier transform infrared spectroscopy (FTIR) of liganded and photoproduct states of oxymyoglobin (MbO_2) and carbonmonoxymyoglobin (MbCO) at cryogenic temperatures reveals a number of modes sensitive to ligation state in the 1050–1150 cm^{-1} region. This region contains contributions from the heme moiety, histidylimidazole side chains, and the dioxygen stretching frequency of MbO_2, all of which are influenced by photolysis and subsequent thermal recombination. For MbCO and MbO_2, we observe modes at 1080 cm^{-1} (designated α) and 1096 cm^{-1} (designated β) that shift to lower frequencies upon photolysis and a third mode (designated γ; in MbCO, 1107 cm^{-1}; in MbO_2, 1105 cm^{-1}) that shifts to a higher frequency upon photolysis. As ligands rebind, these modes revert to their original positions. In addition, we observe an 1115 cm^{-1} mode (designated ϵ) that is unique to compounds in which the iron atom is out of the heme plane. FTIR spectra of apomyoglobin (apo Mb) and heme model compounds: iron(III) octaethylporphyrin (FeOEP), iron(III) chloroprotoporphyrin IX (FePP IX), and $(4MeIm)_2FeOEP$ have aided in the assignment of the α- and β-modes to heme peripheral vinyl groups and the γ-mode to a C–H bending mode of the proximal (His-F8) histidylimidazole. We also present photolysis experiments that support the theory[1] that $\nu(O{=}O)$ couples with a distal and/or proximal histidine mode. The dioxygen stretching frequency appears at 1105 cm^{-1}, overlapping a proximal histidylimidazole C–H bending mode at the same frequency. The frequency shifts we observe in the α-, β-, and γ-modes upon photolysis of the liganded state reflect the changing structural environment of the heme and distal and proximal heme pockets. Thus, those bands are sensitive probes of structural perturbations in hemeproteins. We observe *two* different vinyl deformation bands (α and β), one for each peripheral vinyl group in the heme moiety, arising from unique protein environments. Synchronous, 4 cm^{-1} red shifts of these bands upon photolysis indicate that these modes are sensitive to the electronic changes that are known to occur in the porphyrin π system upon photolysis. The blue shift of the γ-mode may be attributed to changes in the interaction between the heme and proximal histidine upon photolysis, which occurs as the histidine tilts and the iron–histidine bond length shortens.

Introduction

Myoglobin is a heme-containing protein found in muscle tissue; its function is to bind and store oxygen (O_2) when the cellular level is high, and then release the bound O_2 when the cell needs it. More specifically, the oxygen molecule binds to the sixth coordination site of the heme iron, causing conformational changes in the protein, primarily restricted to the distal and proximal heme pockets.[2] Even though a great deal is known about the liganded and deoxy forms of myoglobin, the intermediate conformational states involved in the process of ligand binding are not well understood.

Flash photolysis has been used extensively to study the kinetics of ligand binding and release over a wide range of temperatures.[2] At room temperature, MbCO exhibits bimolecular rebinding kinetics after photolysis of the CO ligand.[2] This type of kinetics indicates a single (observable) protein structure. It is proposed that this structure is composed of a distribution of substates that interconverts at room temperature on a time scale faster than the ligand-rebinding process. At cryogenic temperatures, however, the CO and O_2 rebinding kinetics are nonexponential and independent of ligand concentration, indicating geminate recombination in a heterogeneous system.[3-5] Austin et al. have concluded that the protein is frozen into individual conformational substates from which the CO rebinds, resulting in distinct rebinding kinetics for each conformational substate.[3] Kinetic holeburning data have indicated that a distribution of proximal substates for the photoproduct exerts kinetic control of the rebinding.[6,7] Carbonmonoxymyoglobin (MbCO) has been shown to have structurally distinct substates influenced by structural and electronic perturbations due to the distal pocket.[8-10] These substates have different barriers to recombination.[11,12] A question

* Author to whom correspondence should be addressed.

† Abbreviations used: FTIR, fourier transform infrared spectroscopy; RR, resonance raman spectroscopy; red shift, shift to lower frequency; blue shift, shift to higher frequency; Mb, myoglobin; MbCO, carbonmonoxymyoglobin; MbO_2, oxymyoglobin; Hb, hemoglobin; $Fe^{III}OEP$, iron(III) octaethylporphyrin chloride; $Fe^{III}PP$ IX, iron(III) chloroprotoporphyrin IX; 4MeIm, 4-methylimidazole.

® Abstract published in *Advance ACS Abstracts*, September 15, 1994.

(1) Bruha, A.; Kincaid, J. R. *J. Am. Chem. Soc.* **1988**, *110*, 6006.

(2) Antonini, E.; Brunori, M. *Hemoglobin and myoglobin in their reactions with ligands*; North-Holland: New York, 1971.

(3) Austin, R. H.; Beeson, K.; Eisenstein, L.; Frauenfelder, H.; Gunsalus, I. C. *Biochemistry* **1975**, *14*, 5355.

(4) Doster, W.; Beece, D.; Bowne, S. F.; Dilorio, E. E.; Eisenstein, L.; Frauenfelder, H.; Reinisch, L.; Shyamsunder, E.; Winterhalter, K. H.; Yue, K. T. *Biochemistry* **1982**, *21*, 4831.

(5) Ansari, A.; Berendzen, J.; Bowne, S.; Frauenfelder, H.; Iben, I.; Sauke, T.; Shyamsunder, E.; Young, R. *Proc. Natl. Acad. Sci. U.S.A.* **1985**, *82*, 5000.

(6) Chance, M. R. *Methods in Enzymology* **1993**, *226*, 97.

(7) Campbell, B. F.; Chance, M. R.; Friedman, J. M. *Science* **1987**, *238*, 373.

(8) Makinen, M. W.; Houtchens, R. A.; Caughey, W. S. *Proc. Natl. Acad. Sci. U.S.A.* **1979**, *76*, 6042.

(9) Alben, J. O.; Beece, D.; Bowne, S. F.; Doster, W.; Eisenstein, L.; Frauenfelder, H.; Good, D.; McDonald, J. D.; Marden, M. C.; Moh, P. P.; Reinisch, L.; Reynolds, A. H.; Shyamsunder, E.; Yue, K. T. *Proc. Natl. Acad. Sci. U.S.A.* **1982**, *79*, 3744.

(10) Hong, M. K.; Braunstein, D.; Cowen, B.; Frauenfelder, H.; Iben, I. E. T.; Mourant, J. R.; Ormos, P.; Scholl, R.; Schulte, A.; Steinback, P. J.; Xie, A.; Young, R. D. *Biophys. J.* **1990**, *58*, 429.

(11) Ansari, A.; Berendzen, J.; Braunstein, D.; Cowen, B. R.; Fraunfelder, H.; Hong, M. K.; Iben, I. E. T.; Johnson, J. B.; Ormos, P.; Sauke, T. B.; Scholl, R.; Schulte, A.; Steinbach, P. J.; Vittitow, J.; Young, R. D. *Biophys. Chem.* **1987**, *26*, 337.

(12) Chance, M. R.; Campbell, B. F.; Hoover, R.; Friedman, J. M. *J. Biol. Chem.* **1987**, *262*, 6959.

0002-7863/94/1516-9662$04.50/0

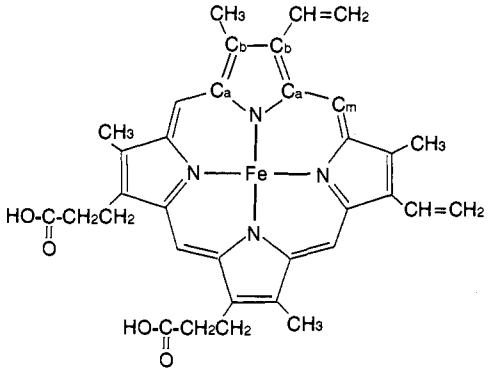

Figure 1. Structure of iron(III) protoporphyrin IX (Fe^{III}PP IX), with atom labeling. In iron(III) octaethylporphyrin (Fe^{III}OEP), all of the C_b substituents are replaced by ethyl groups.

of importance is the significance of these substates to oxymyoglobin (MbO_2).[13-15]

Carbon monoxide (CO) binding has been used as a model for oxygen binding, but a number of studies have shown that O_2 and CO have significantly different rebinding intermediates.[4,16] For example, it is thought that bound oxygen in MbO_2 forms a hydrogen bond with the distal histidine, a feature which is absent in MbCO.[1,17-19] Also, the quantum yield of photolysis of MbCO was found to be 1.0 and only 0.03 for MbO_2 on the microsecond time scale.[2] However, Chance et al.[16] have shown that, on 30 ps to long time scales at cryogenic temperatures, the photolysis quantum yield of MbO_2 is 0.4 and that of MbCO is 1.0. Thus, below 10 K, 40% of MbO_2 molecules can be converted to stable photoproduct, while MbCO can be fully converted to a "deoxy-like" state. These stable photoproducts can be reconverted to the fully liganded form by warming to 100–120 K.[6] The discrepency between the microsecond and picosecond quantum yields in MbO_2 has been attributed to geminate recombination that occurs on 100 ns and longer time scales.[2,16,20,21] There is a 60% fraction of MbO_2 molecules that either (1) do not photolyze or (2) photolyze and recombine on a time scale shorter than 30 ps.[16] In either case, the result reveals a profound difference between the ligand-rebinding pathways in MbCO and MbO_2.

Vibrational spectroscopy is an excellent tool for probing changes in the heme pocket associated with ligand binding and release. It can be used to study MbCO and MbO_2 independently and directly. More specifically, the infrared region between 1050 and 1150 cm^{-1} provides a wealth of information about the heme moiety, histidylimidazole side chains, and the dioxygen stretching frequency of MbO_2, all of which are affected by photolysis.

Myoglobin's porphyrin component is protoporphyrin IX (Figure 1), which has been shown by infrared and resonance Raman (RR) spectroscopy to contain both skeletal and vinyl modes in the 1050–1150 cm^{-1} infrared region.[22,23] Since the vinyl groups are located at the periphery of the porphyrin ring, these modes are quite sensitive to their environments, making specific contacts with the globin moiety[23,24] and thus provide excellent structural markers of ligand rebinding intermediates.

RR spectroscopy of free imidazole, free histidine, and poly(L-histidine) has demonstrated that internal modes of the histidine side chain also fall in the 1050–1150 cm^{-1} region of the infrared spectrum.[25,26] Additionally, redox-sensitive modes attributed to the heme–histidine complex have been identified around 1100 cm^{-1} in myoglobin[27] and cytochrome $b559$[28] by FTIR difference spectroscopy. So, analysis of this region not only provides information on the heme moiety but it also may reveal structural details regarding histidine residues in the protein, notably the distal (His-E7) and/or the proximal (His-F8) histidines.

RR and FTIR spectroscopy have been successful in directly probing the vibrational modes associated with the Fe–O_2 linkage, which also falls between 1050 and 1150 cm^{-1}.[1,29-32] FTIR difference spectroscopy of isotopically labeled $Mb^{18}O_2$, $Mb^{17}O_2$, and $Mb^{16}O_2$ has been used to identify several O_2 stretching bands that were tentatively assigned to oxymyoglobin conformational substates.[31] Kincaid and co-workers[1,32] greatly elaborated on the work of Potter et al.[31] by studying the effects of solvent variation and O_2 isotopic substitution on RR spectra of cobalt-substituted myoglobin, various hybrid cobaltous hemoglobins, and several cobalt porphyrin complexes with trans-axial bases.[1,32] The authors obtained a similar multiple-band pattern but attributed the appearance of multiple O_2 bands to the vibrational coupling of bound dioxygen to internal modes of the proximal or distal histidylimidazole.

To date, vibrational spectroscopic studies between 1050 and 1150 cm^{-1} have all been performed on bound MbO_2 and MbCO. In this paper, we present the results of low-temperature FTIR experiments of *liganded* and *photolyzed* MbO_2 and MbCO. By examining this infrared region, experiments such as these can probe (1) heme structural changes that result from photolysis of liganded myoglobin, (2) protein conformational changes that occur upon photolysis, notably those involving the distal and/or proximal histidines, and (3) the location of the iron-bound ν(O=O), a signal which is expected to decrease upon photolysis of the O_2 ligand.

Experimental Section

Horse skeletal muscle myoglobin (95–100%), deuterium oxide (99.9%), and trizma base were purchased from Sigma Chemical Co. Sodium dithionite and hydrochloric acid (36.5–38%) were purchased from J. T. Baker & Co. Potassium bromide, 4-methylimidazole (4MeIm), iron(III) 2,3,7,8,12,13,17,18-octaethyl-21*H*,23*H*-porphyrin chloride (Fe^{III}OEP), and iron(III) chloroprotoporphyrin IX (Fe^{III}PP IX) were purchased from Aldrich Chemical Co. Dichloroethane was purchased from Kodak. Carbon monoxide (99.5 atom %) and O_2 (99 atom %) were purchased from MG Industries. All chemicals and gases were used without further purification.

A. Preparation of Solid Porphyrin Samples and Recording of Their FTIR Spectra. FTIR spectra of Fe^{III}OEP, Fe^{III}PP IX, 4MeIm, and $(4MeIm)_2Fe^{III}$OEP were obtained on solid samples. N-Deuterated 4-methylimidazole was prepared as described previously.[33] Crystals of $(4MeIm)_2Fe^{III}$OEP were prepared by adding excess 4MeIm or N-deuterated 4MeIm to Fe^{III}OEP in 1,2-dichloroethane and evaporating the solution to dryness.

(13) Caughey, W. S.; Shimada, H.; Choc, M. G.; Tucker, M. P. *Proc. Natl. Acad. Sci. U.S.A.* **1981**, *78*, 2903.
(14) Tsubaki, M.; Yu, N.-T. *Proc. Natl. Acad. Sci. U.S.A.* **1981**, *78*, 3581.
(15) Potter, W. T.; Hazzard, J. H.; Choc, M. G.; Tucker, M. P.; Caughey, W. S. *Biochemistry* **1990**, *29*, 6283.
(16) Chance, M. R.; Courtney, S. H.; Chavez, M. D.; Ondrias, M. R.; Friedman, J. M. *Biochemistry* **1990**, *29*, 5537.
(17) Pauling, L. *Nature* **1964**, *203*, 182.
(18) Phillips, S. E. V. *J. Mol. Biol.* **1980**, *142*, 531.
(19) Lee, H. C.; Ikeda-Saito, M.; Yonetani, T.; Maggliozo, R. S.; Peisach, J. *Biochemistry* **1992**, *31*, 7274.
(20) Alpert, B.; Mohsni, S. E.; Lindquist, L.; Tfibel, F. *J.Chem. Phys.* **1979**, *64*, 11.
(21) Friedman, J. M.; Lyons, K. B. *Science* **1980**, *284*, 570.
(22) Choi, S.; Spiro, T. G.; Langry, K. C.; Smith, K. M. *J. Am. Chem. Soc.* **1982**, *104*, 4337.
(23) Choi, S.; Spiro, T. G.; Langry, K. C.; Smith, K. M.; Budd, D. L.; LaMar, G. N. *J. Am. Chem. Soc.* **1982**, *104*, 4345.
(24) Campbell, B. F.; Chance, M. R.; Friedman, J. M. *J. Biol. Chem.* **1987**, *262*, 14885.
(25) Ashikawa, I.; Itoh, K. *Biopolymers* **1979**, *18*, 1859.
(26) Salama, S.; Spiro, T. G. *J. Am. Chem. Soc.* **1978**, *100*, 1105.
(27) Schlereth, D. D.; Mantele, W. *Biochemistry* **1992**, *31*, 7494.
(28) Berthomieu, C.; Boussac, A.; Mantele, W.; Breton, J.; Nabedryk, E. *Biochemistry* **1992**, *31*, 11460.
(29) Barlow, C. H.; Maxwell, J. C.; Wallace, W. J.; Caughey, W. S. *Biochem. Biophys. Res. Commun.* **1973**, *55*, 91.
(30) Maxwell, J. C.; Volpe, J. A.; Barlow, C. H.; Caughey, W. S. *Biochem. Biophys. Res. Commun.* **1974**, *58*, 166.
(31) Potter, W. T.; Tucker, M. P.; Houtchens, R. A.; Caughey, W. S. *Biochemistry* **1987**, *26*, 4699.
(32) Proniewicz, L. M.; Kincaid, J. R. *J. Am. Chem. Soc.* **1990**, *112*, 675.
(33) Sundberg, R. J.; Martin, R. B. *Chem. Rev.* **1974**, *74*, 471.

Pellets (10 mm diameter × 1 mm thickness) were prepared by mixing 5 mg of sample and 100 mg of KBr in a mortar and pestle and then pressing the mixture in a Spectra Tech Econo-Press. Spectra were obtained with a Mattson Galaxy Series 5000 FTIR equipped with a liquid-nitrogen cooled MCT detector and interfaced to a Gateway 386 computer. For each spectrum, 512 scans were taken at a 2 cm^{-1} resolution and ratioed to air.

B. Preparation of Myoglobin Samples. Apomyoglobin was prepared as described previously.[34] For MbCO and MbO_2 samples, horse myoglobin was dissolved in buffer (200 mM tris/D_2O, pH 7.0) and stirred on ice for 10 min. Samples were then centrifuged for 20 min at 10 °C at 15 000 rpm. After centrifuging, samples were decanted into a test tube and stirred on ice in a nitrogen-atmosphere drybox. A 5-fold excess of sodium dithionite was added to reduce all of the iron to the Fe^{II} state. After stirring 10 more min, oxygen (O_2) or carbon monoxide (CO) gas was continuously blown over the sample for 10 min to generate oxy- or carbonmonoxymyoglobin. Samples were pipetted into the FTIR cell, and a UV–visible spectrum of the loaded FTIR cell revealed the sample to be greater than 95% oxy- or carbonmonoxymyoglobin.

C. Recording of Myoglobin FTIR Spectra in Solution. Infrared spectra were obtained with a Mattson Galaxy Series 5000 FTIR equipped with a liquid-nitrogen cooled MCT detector and interfaced to a Gateway 386 computer. For each spectrum, 128 scans were taken at a 2 cm^{-1} resolution.

Samples were placed between CaF_2 windows (2 mm thick) with a 0.025 mm Teflon spacer. (Windows and spacers were purchased from Spectra-Tech.) The sample cell was mounted to the base of the cold finger in a low-temperature cryostat (Janis Model ST-4-B). A silicon diode thermocouple was mounted just below the sample. Samples were initially frozen by cooling the cryostat to 200 K with liquid helium using a liquid helium transfer line. Then, the cryostat was evacuated to 10 mTorr, and the temperature was slowly lowered to 120, 70, 50, 30, and 10 K. Spectra of the unphotolyzed sample were taken at these respective temperatures. Once the 10 K unphotolyzed spectrum was taken, the sample was photolyzed for 5 min on each side with a high-intensity white light source (CUDA Products, Inc. Model I-150). Photolysis raised the sample temperature by no more that 2 K, and all photolysis was performed at 10 K. After photolysis, the sample was warmed by reducing the liquid helium flow and heating the sample via a heating wire mounted on the cryostat cold finger and interfaced to a Lakeshore Temperature Controller (Model no. 805). Spectra of the photolyzed sample were taken at 10, 30, 50, 70, and 120 K.

Spectral interferograms were collected and fourier transformed using FIRST software provided by Mattson Inc. For the second derivative spectra, the photolyzed and unphotolyzed spectra were referenced to air spectra and then converted from transmittance to absorbance units. For difference spectra, photoproduct spectra were ratioed to liganded spectra at each respective temperature and then converted from transmittance to absorbance units. Spectra were then imported into Spectra Calc software (Galactic Industries, Nashua, NH) for all further data analysis.

As has been discussed extensively by Caughey and co-workers,[31] the region of the infrared spectrum between 1050 and 1150 cm^{-1} is swamped by protein and solvent absorption. Therefore, significant spectral changes that occur in this region upon photolysis of MbCO or MbO_2 are buried within the background infrared absorbance of the sample and solvent. Steps were taken to minimize the background and maximize the photolysis quantum yield of the sample. For cryogenic experiments, glycerol is usually the solvent of choice because it freezes as a glass. However in the 1050–1150 cm^{-1} region, glycerol has a high absorbance. D_2O was chosen over H_2O because it absorbs less in this region.[35] Sample pathlength and concentration were adjusted to provide an overall absorbance of ~0.2 OD in the visible region (542 nm), in order that an adequate photolysis level could be attained. An estimation was made of photolysis quantum yields for the MbCO spectra by comparing the absorbance at $\nu(C{\equiv}O)$ (1945 cm^{-1}) for the 10 K photoproduct spectrum to the absorbance at the same frequency for the 10 K liganded spectrum. Unlike MbCO, MbO_2 spectra do not contain a strong, unperturbed O_2 band as a marker for photolysis. Therefore, the photolysis quantum yield of the MbCO spectra was maximized, and the same photolysis protocol was used for MbO_2.

(34) Teale, F. W. J. *Biochim. Biophys. Acta* **1959**, *35*, 543.
(35) Caughey, W. S. In *Methods for determining metal ion environments in proteins: Structure and function of metalloproteins*; Darnall, D. W., Wilkins, R. G., Eds.; Elsevier: North-Holland, New York, 1980; p 95.

Results

Techniques such as difference spectra, fourier deconvoluted spectra, and derivative spectra have evolved as methods to filter out the high background often observed in the FTIR spectra of biological samples, thus revealing modes that would otherwise be hidden. Recently for myoglobin studies, difference FTIR spectroscopy has been used to study $\nu(O{=}O)$ in isotopically labeled MbO_2 samples[31] and also in an elegant comparison of met Mb to deoxy Mb.[27] Derivative and Fourier deconvoluted methods have been used in numerous studies in order to probe protein conformational changes.[36–41] Review articles by Mantsch and co-workers[42–44] and Nakamato and Czernuszewicz[45] detail the potential, limitations, and applications of these resolution-enhancement techniques to infrared spectra of biological samples. The nature of our experimental protocol has enabled us to generate *both* difference spectra and second derivative spectra as complementary ways of observing the spectral changes that occur in this region upon photolysis and our data illustrate the advantages and disadvantages of each.

A. Analysis of Liganded and Photoproduct MbCO Spectra: Difference Spectroscopy. A 10 K MbCO difference spectrum is obtained by ratioing the photoproduct MbCO spectrum at 10 K to the liganded MbCO spectrum at 10 K, i.e., Mb*CO (10 K)/MbCO (10 K), and baselining the resultant spectrum with a cubic polynomial. Similar difference spectra are obtained at 30, 50, and 70 K. The results are shown in Figure 2A. The positive and negative peaks represent characteristics of the photoproduct and liganded species, respectively. Photoproduct modes occur at 1075, 1091, 1111, and 1115 cm^{-1}. Liganded modes fall at 1080, 1096, and 1105 cm^{-1}. As the sample recombines, the differences between MbCO and Mb*CO are reduced.

In this study for MbCO and MbO_2, we are able to control pathlength, concentration, temperature, and ligand saturation accurately because we are ratioing liganded and photoproduct states of the *same* sample at a given temperature before and after photolysis. Using this difference technique, the Mattson FTIR instrument produces absorbance noise on the order of 10^{-5} OD units. Therefore, absorbance differences of 0.001 OD units or more in the myoglobin spectra result in high quality spectral bands. Difference spectra such as these are advantageous over the raw spectra because the background protein and solvent, which remain unaffected by photolysis, are divided out, thus accentuating the *differences* between the liganded MbCO and its photoproduct.

B. Analysis of Liganded and Photoproduct MbCO Spectra: Second Derivative Spectroscopy. Second derivative spectra are generated by ratioing each photoproduct or liganded spectrum to air, converting to absorbance, and taking the second derivative—no baseline fitting was used to generate this set of spectra. This procedure was used to generate second derivatives of liganded MbCO at 10 K, and photolyzed MbCO at 10, 30, 50, and 70 K and these spectra can be seen in Figure 3. One must keep in mind that any positive peaks in the raw spectrum will

(36) Yamagishi, T.; Ebina, F.; Yamauchi, F. *Agric. Biol. Chem.* **1982**, *46*, 2441.
(37) Ichikawa, T.; Terada, H. *Biochim. Biophys. Acta* **1981**, *671*, 33.
(38) Ruckpaul, K.; Rein, H. *Acta. Biol. Med. Ger.* **1980**, *39*, 55.
(39) Ruckpaul, K.; Rein, H.; Ballon, D. P.; Coon, M. J. *Biochim. Biophys. Acta* **1980**, *626*, 41.
(40) Ichikawa, T.; Terada, H. *Biochim. Biophys. Acta* **1979**, *580*, 120.
(41) Demchenko, A. P. *Dopov. Akad. Sci. Ukr. Ser. B (USSR)* **1978**, *4*, 359.
(42) Mantsch, H. H. In *Spectroscopy of Inorganic Bioactivators: Theory and Applications—Chemistry, Physics, Biology, and Medicine*; Theophanides, T., Ed.; Kluwer Academic Publishers: Boston, 1989; p 307.
(43) Surewicz, W. K.; Mantsch, H. H. *Biochim. Biophys. Acta* **1988**, *952*, 115.
(44) Mantsch, H. H.; Casal, H. L.; Jones, R. N. In *Spectroscopy of Biological Systems*; Clark, R. J. H., Hester, R. E., Eds.; Wiley: New York, 1986; p 1.
(45) Nakamoto, K.; Czernuszewicz, R. S. *Methods Enzymol.* **1993**, *226*, 259.

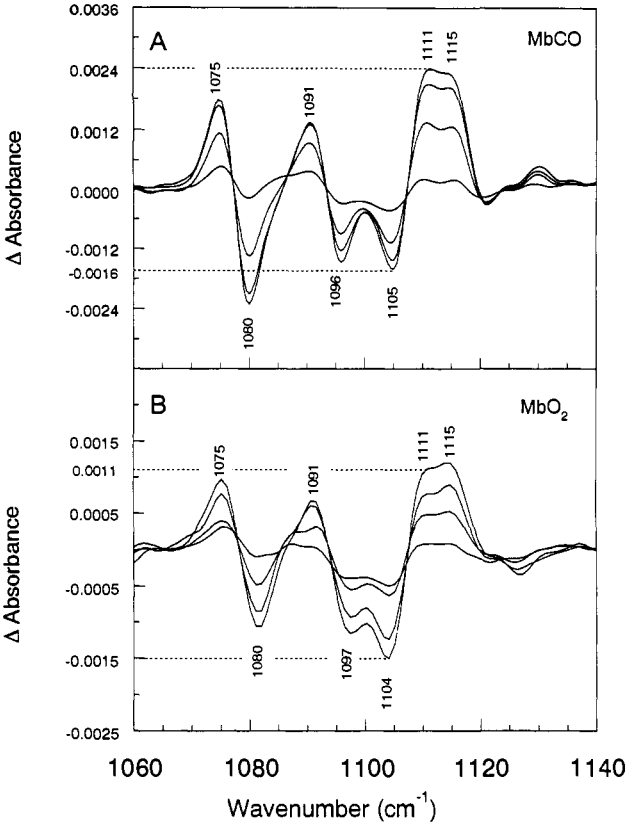

Figure 2. Difference FTIR spectra of (A) MbCO and (B) MbO_2. Spectra were generated by ratioing the photoproduct MbCO (MbO_2) spectrum by the liganded MbCO (MbO_2) spectrum at 10, 30, 50, and 70 K and baselining the resultant spectra with a cubic polynomial. The MbCO sample was 2.6 mM, pH 6.3. The MbO_2 sample was 4.3 mM, pH 6.0. The sample thickness was 0.0025 cm. Both samples were photolyzed at 10 K for 5 min per side with a high-intensity white light source. For each spectrum, 128 scans were taken at 2 cm^{-1} resolution.

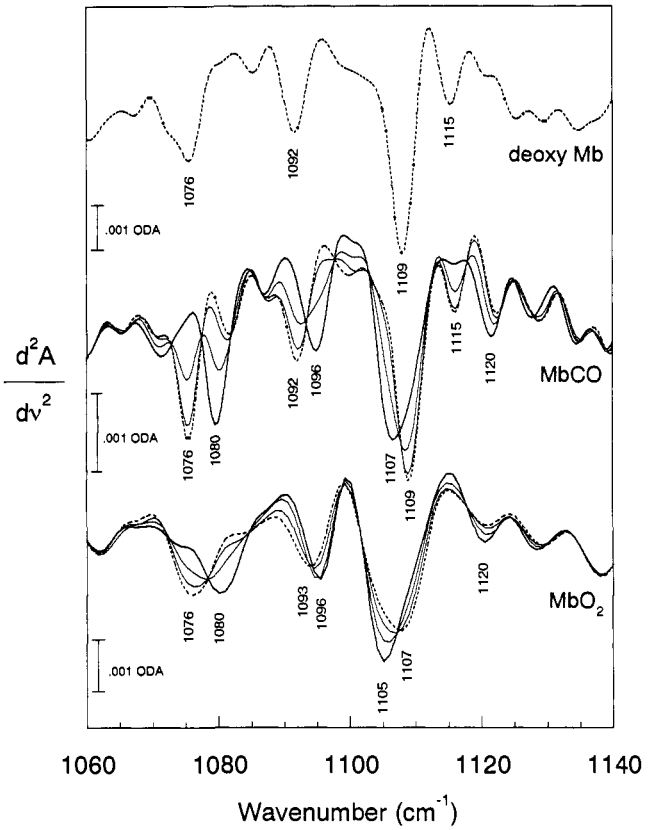

Figure 3. Second derivative FTIR spectra of deoxy Mb at 10 K (- -); liganded MbCO at 10 K (—), the MbCO photoproduct at 10 K (- -), 30 K (—), and 50 K (—); and liganded MbO_2 at 10 K (—), the MbO_2 photoproduct at 10 K (- -), 30 K (—), and 50 K (—). Data are the same as those collected for Figure 2. Spectral units are absorbance acceleration (ODA).

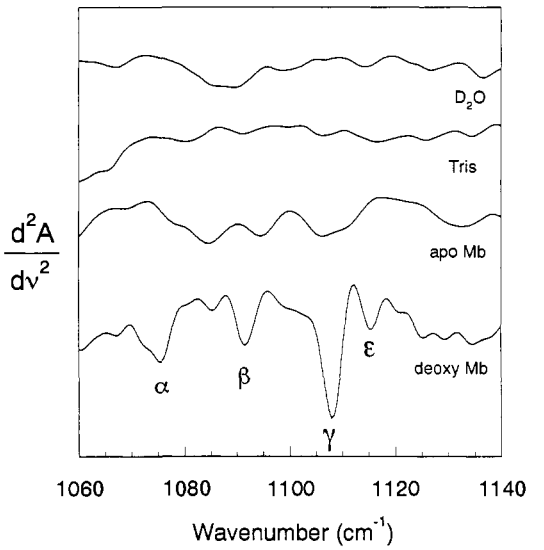

Figure 4. Second derivative FTIR spectra at 70 K of D_2O: tris buffer, pH 7.0, 250 mM; apo Mb, pH 6.0, 3.9 mM in D_2O; and deoxy Mb, pH 6.5, 5.4 mM in D_2O. For each spectrum, 128 scans were taken at 2 cm^{-1} resolution.

appear as negative peaks in the second derivative spectrum and vice versa. The striking features in the second derivative spectrum of 10 K, liganded MbCO are modes at 1080, 1096, 1107, and 1120 cm^{-1}. The 10 K photoproduct spectrum has major bands at 1076, 1092, 1109, 1115, and 1120 cm^{-1}. These are the same liganded and photoproduct modes that appear in the MbCO difference spectra except for the 1120 cm^{-1} mode, which is not resolved in the difference spectra.

The important thing to note is that the second derivative spectra of Mb*CO at 30, 50, and 70 K provide additional information that is not revealed to the same extent in the difference spectra; they show the *evolution* of Mb*CO modes to MbCO modes as the sample recombines, i.e., the 1076 cm^{-1} photoproduct mode shifts to 1080 cm^{-1} with an isosbestic point at 1078 cm^{-1} (and this mode has been designated α), the 1092 cm^{-1} photoproduct mode shifts to 1096 cm^{-1} with an isosbestic point at 1094 cm^{-1} (designated β), there is a partial shift and decreased intensity in the photoproduct mode at 1109 to 1107 cm^{-1} (designated γ), a mode (designated ϵ) at 1115 cm^{-1} disappears, and there is a shift and increase in intensity of the band (designated ζ) at 1120 cm^{-1}.

Second derivative spectroscopy is superior to difference spectroscopy when comparing two samples, i.e., deoxy Mb and MbCO or Mb*CO (Figure 3). As can be seen, the Mb*CO spectrum is essentially the same as deoxy Mb with respect to the α-, β-, γ-, and ϵ-bands. The liganded mode at 1080 cm^{-1} (α-band) shifts to 1076 cm^{-1} in the photoproduct, 1076 cm^{-1} being the location of a pure deoxy-like band. The case is the same for the liganded 1096 (β) and 1107 cm^{-1} (γ) bands that shift to deoxy-like positions of 1092 and 1109 cm^{-1}, respectively. Additionally, a deoxy-like band appears in the photoproduct spectrum at 1115 cm^{-1} (ϵ-band). This feature is entirely absent in the liganded spectrum.

The major disadvantage of second derivative spectra is that all sharp (and often weak) features are accentuated by this technique,[43] meaning that contributions from all modes of the protein and solvent are present. Therefore, control spectra are essential (i.e., solvent, buffer) (Figure 4). Also, it is advantageous to *compare* second derivative spectra; in this case we identify only those modes that *change* peak position or intensity upon

photolysis, thus identifying the photolysis-sensitive modes with functional processes in myoglobin and ruling out contributions of the protein background, buffer, or solvent.

C. Difference Spectra and Second Derivative Spectra of Liganded and Photoproduct MbO_2. When oxygen is used as the myoglobin ligand, the spectra become more complicated due to the presence of the ν(O=O) in the 1050–1150 cm^{-1} region.[31] Figure 2B shows the 10 K difference (photoproduct/liganded) FTIR spectra of MbO_2. Liganded and photoproduct modes fall in similar positions in the oxymyoglobin spectra as in they do in MbCO. Overall the spectra look very similar, but the most notable difference is in the intensities of the liganded γ-mode. Taking the liganded β-mode (1096 cm^{-1}) as a reference, the γ-mode intensity is significantly greater in MbO_2 than MbCO.

Figure 3 shows the second derivative FTIR spectra of liganded MbO_2 and the 10, 30, and 50 K MbO_2 photoproducts. The narrowed bandwidths of these spectra provide details unattainable from the difference spectra. When comparing the 10 K liganded spectra of MbO_2 to MbCO, the α and β bands fall at 1080 and 1096 cm^{-1}, respectively, just like MbCO. The γ band at 1107 cm^{-1} in MbCO falls at 1105 cm^{-1} in MbO_2. In the oxymyoglobin photoproduct, the α and β band intensities only partially shift to deoxy-like positions, due to the 40% quantum yield of MbO_2 photolysis at cryogenic temperatures. The γ mode decreases in intensity and shifts from 1105 to 1107 cm^{-1}.

Finally, it is important to note that as the ligand rebinds upon warming of the sample, all spectral changes that occur upon photolysis are completely reversible; second derivative FTIR spectra of all samples warmed to 70 K after photolysis are identical to the 10 K liganded (prephotolysis) spectra (data not shown).

Discussion

MbCO Spectra and the Assignment of Protein and Heme Modes That Are Sensitive to Photolysis. It has been well established that ν(C≡O) occurs between 1930 and 1970 cm^{-1} in hemeproteins.[46] The Fe–C bond stretch is observed at ~515 cm^{-1} and the Fe—C≡O bend is seen at ~580 cm^{-1}.[47] Therefore, the infrared region between 1050 and 1150 cm^{-1} is void of any Fe—C≡O vibrations. So, the α, β, γ, and ϵ bands must be protein and/or heme modes that are structurally or electronically sensitive to ligand photolysis.

A. Protein Backbone Modes. Difference spectra of electrochemically generated oxidized (met Mb) and reduced (deoxy Mb) myoglobin reveal modes of the protein backbone, protein side chains, and the porphyrin moiety which are sensitive to the redox process.[27] In the same way, we find that the α-, β-, γ-, and ϵ-modes are sensitive to ligand photolysis and thus may be due to any of the above mentioned modes of the myoglobin structure.

To help distinguish between protein and porphyrin modes, we have studied apomyoglobin (i.e., the heme group has been removed) and several porphyrin model compounds (i.e., the protein has been removed). IR spectroscopy has been used to show that the secondary structure of myoglobin changes minimally upon removal of the heme group.[48] However, some differences can be seen through comparison of the amide regions of the FTIR spectra of apo Mb and MbCO (data not shown), yet the overall fingerprint from 1200–1900 cm^{-1} is similar. Alternatively, the 1050–1150 cm^{-1} region of these two spectra is quite different. At equal concentrations and pathlengths, some absorption due to the protein backbone is present, but the α, β, γ, and ϵ modes are not visible in the apo Mb spectrum (Figure 4). This result implies that these photolysis-sensitive modes are not markers of the protein backbone structure but are more likely modes of the porphyrin ring itself or protein side chain modes involved in the coordination of the heme moiety to the globin component.

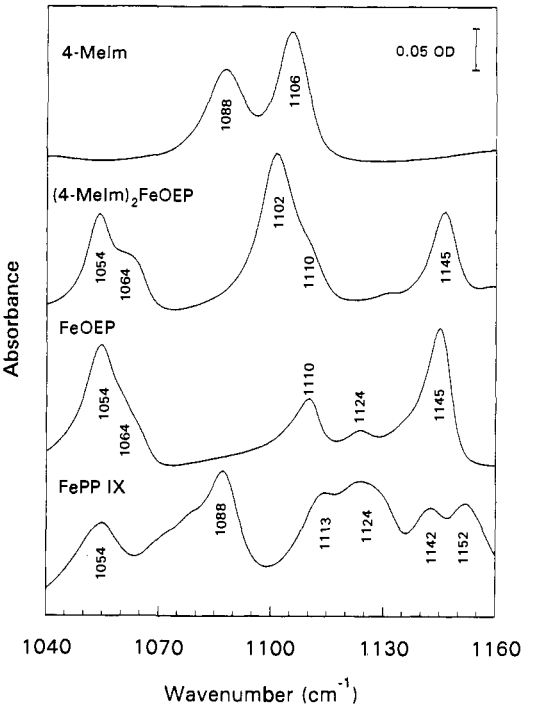

Figure 5. Raw (ratioed only to air) FTIR spectra of 4-MeIm, $(4MeIm)_2Fe^{III}OEP$, $Fe^{III}OEP$, and $Fe^{III}PP$ IX at room-temperature. Spectra were taken on solid samples pressed with KBr into 1 mm thick pellets. For each spectrum, 512 scans were taken at 2 cm^{-1} resolution.

B. Porphyrin Modes. Previous RR and FTIR studies on various porphyrin compounds have assigned both skeletal (C_a–N, C_a–C_b, C_a–C_m, C_b–C_b, C_b–C_m) and peripheral vinyl (C_b—CH=CH_2) modes to the 1050–1150 cm^{-1} region of the infrared spectrum (Figure 1).[22,23,49] FTIR studies presented here on model iron porphyrin compounds (Figure 5) corroborate these results.

Full assignment has been made of fundamental (1121 cm^{-1}, C_a–N; 1159 cm^{-1}, C_b–S) and combination (1138 cm^{-1}, $C_aC_mC_a$ + C_b–S) {S = point mass substituents} Raman skeletal modes of nickel octaethylporphyrin ($Ni^{II}OEP$).[49] Infrared spectra of the same compound reveal additional fundamental skeletal modes (1057 cm^{-1}, C_b–S; 1113 cm^{-1}, C_b–S; 1148 cm^{-1}, C_b–S).[22,49] Raman spectra of $Im_2Fe^{II}PP$ IX and $Im_2Fe^{III}PP$ IX also display a similar skeletal mode pattern.[23] Figure 5 shows the FTIR spectra of iron(III) octaethylporphyrin ($Fe^{III}OEP$). Similar to $Ni^{II}OEP$, $Fe^{II}PP$ IX, and $Fe^{III}PP$ IX, we observe pronounced porphyrin skeletal modes at 1054 cm^{-1} (C_b–S), 1110 cm^{-1} (C_b–S), 1124 cm^{-1} (C_a–N), and 1145 cm^{-1} ($C_aC_mC_a$ + C_b–S).

Two of the C_b positions on the porphyrin moiety in myoglobin, iron protoporphyrin IX ($Fe^{II}PP$ IX), contain peripheral vinyl modes, which themselves have active Raman and infrared modes in the 1050–1150 cm^{-1} region.[22,23] The Raman spectra of $Ni^{II}PP$ IX, $Im_2Fe^{II}PP$ IX, and $Im_2Fe^{III}PP$ IX each contain a vinyl mode at 1089 cm^{-1} (=CH_2 deformation) in addition to perturbed skeletal modes at 1130 ($C_aC_mC_a$ + C_b–S) and 1125 cm^{-1} (C_a–N). The infrared spectrum of $Ni^{II}PP$ IX has a vinyl mode at 1080 cm^{-1} (=CH_2 deformation) and a ring-vinyl stretch (C_b—CH=CH_2) at 1118 cm^{-1}. The infrared spectrum of iron(III) chloroprotoporphyrin IX ($Fe^{III}PP$ IX) (Figure 5) has a peripheral vinyl mode at 1088 cm^{-1} (=CH_2 deformation) and a band at 1113 cm^{-1} assignable to a ring-vinyl stretch (C_b—CH=CH_2), in addition to the porphyrin skeletal modes at 1054 cm^{-1} (C_b–S), 1124 cm^{-1} (C_a–N), and 1142 cm^{-1} (C_b–S).

Comparison of the second derivative and difference FTIR spectra of MbCO to the heme model compound spectra suggests

(46) Alben, J. O.; Caughey, W. S. *Biochemistry* **1968**, *7*, 175.
(47) Tsubaki, M.; Srivastava, R. B.; Yu, N. T. *Biochemistry* **1982**, *21*, 1132.
(48) Jacobson, A. L.; Krueger, P. J. *Biochim. Biophys. Acta* **1975**, *393*, 274.
(49) Kitagawa, T.; Abe, M.; Ogoshi, H. *J. Chem. Phys.* **1978**, *69*, 4516.

Table 1. Summary of Frequencies and Assignments of Photolysis-Sensitive Myoglobin Bands and Corresponding Model Compound Bands in the 1050–1150 cm^{-1} Infrared Region

	α	β	γ	ϵ	ζ
$MbCO_{liganded}$	1080[b]	1096[b]	1107[c]		1120[a]
$MbCO_{photoproduct}$	1076[b]	1092[b]	1109[c]	1115[e]	1122[a]
$MbO_{2liganded}$	1080[b]	1096[b]	1105[d]		1120[a]
$MbO_{2photoproduct}$	1076[b]	1094[b]	1107[d]	1115[e]	1120[a]
deoxy Mb	1076[b]	1092[b]	1109[c]	1115[e]	1120[a]
Fe^{III}PP IX		1088[b]		1113[e]	1124[a]
Fe^{III}OEP				1110[a]	1124[a]
4MeIm			1106[c]		
$(4MeIm)_2Fe^{III}$OEP			1102[c]	1110[e]	1123[a]

[a] Heme skeletal mode. [b] Heme peripheral mode. [c] Histidylimidazole C–H bending mode. [d] O=O stretch overlapped by a histidylimidazole C–H bending mode. [e] Ring-vinyl stretch.

assignment of the α, β, ϵ, and ζ bands to modes of heme moiety (Table 1). The intense peripheral vinyl mode in Fe^{III}PP IX at 1088 cm^{-1} falls directly between the α (liganded, 1080 cm^{-1}) and β (liganded, 1096 cm^{-1}) modes in the MbCO spectra. Therefore, we propose that the α and β modes are assignable to vinyl $=CH_2$ deformations. It has been shown that heme protein modes that involve C_b-substituents on the heme (peripheral vinyl and/or propionic acid groups) are quite sensitive to their environments, i.e., specific globin contacts.[23,24] For this reason, we observe *two* different vinyl $=CH_2$ deformation bands (α and β bands), one for each peripheral vinyl group in the heme moiety, arising from unique protein environments. Frequency shifts of these bands upon photolysis are additional evidence that these modes are extremely sensitive to changes in their environments. Future studies with distal and proximal heme pocket mutants will be useful in addressing then structural/electronic nature of these individual environments.

The 1115 cm^{-1} (ϵ) MbCO photoproduct band can be assigned to a ring-vinyl stretch (C_b—CH=CH_2). A similar band has been assigned as such in $Mb^{III}F$ (1124 cm^{-1}) and deoxy Mb (1117 cm^{-1}) by Raman spectroscopy.[23] This mode correlates to the 1113 cm^{-1} mode of Ni^{II}OEP, which shifts to 1118 cm^{-1} in Ni^{II}PP IX and falls at 1113 cm^{-1} in Fe^{III}PP IX. The 1120 cm^{-1} ζ band corresponds to the skeletal modes at 1124 cm^{-1} in Fe^{III}OEP and Fe^{III}PP IX.

C. Protein Side Chain Modes. The remaining unassigned mode of the MbCO spectra (γ band) is not assignable to a porphyrin mode but to a photolysis-sensitive mode of the protein. This mode is not a conformational marker of the protein backbone because removal of the heme from the protein (i.e., apomyoglobin) causes a disappearance of the γ-mode (Figure 4). It is plausible that removal of the heme could alter modes of the heme pocket amino acid side chains. The only amino acid side chain that absorbs in this region is the imidazole side chain of histidine. It has been shown that other aromatic amino acid side chains do not have pronounced vibrational modes between 1050 and 1150 cm^{-1}.[50] Myoglobin contains two essential histidines that are known to experience conformational changes upon photolysis, namely the distal (His-E7) and the proximal (His-F8) histidines.

RR spectroscopy has been used to identify C–H bending modes in the 1050–1150 cm^{-1} region of the infrared spectrum in imidazole (1070 and 1100 cm^{-1}),[26] 4-methylimidazole (1092 and 1107 cm^{-1}),[1] free histidine (1103 cm^{-1}), and poly(L-histidine) (1110 cm^{-1}).[25] The FTIR spectrum of 4-methylimidazole (the imidazole derivative most resembling the histidine side chain) reveals similar C–H bending modes at 1088 and 1106 cm^{-1} (Figure 5A). Since the myoglobin studies were done in D_2O (where histidine N–H's are deuterated), it must be noted that N-deuteration of 4-methylimidazole does not affect its FTIR spectrum between 1050 and 1150 cm^{-1}.

The issue of whether the γ-mode is due to the distal and/or proximal histidine is addressed by studying the coordination of 4-methylimidazole (4MeIm) to Fe^{III}OEP. The FTIR spectrum of coordinated 4MeIm differs from that of the free compound; upon coordination of 4MeIm to Fe^{III}OEP (Figure 5), the two C–H bending modes of uncoordinated 4MeIm are reduced to a single, intense mode at 1102 cm^{-1} in $(4MeIm)_2Fe^{III}$OEP, comparable to the single intense γ-mode at 1107 cm^{-1} in MbCO. The remaining bands in the $(4MeIm)_2Fe^{III}$OEP spectrum are attributable to porphyrin skeletal modes of Fe^{III}OEP. (Coordination of N-deuterated 4MeIm does not affect the spectrum of $(4MeIm)_2Fe^{III}$OEP between 1050 and 1150 cm^{-1}.)

Redox-sensitive modes attributed to the heme–histidine complex have already been identified in cytochrome *b*559 (reduced cyt *b*559, 1104 cm^{-1})[28] and in myoglobin (reduced Mb, 1106 cm^{-1}; oxidized Mb, 1100 cm^{-1})[27] by FTIR difference spectroscopy. We also observe a shift in the γ-mode from reduced Mb (1109 cm^{-1}) to oxidized Mb (1103 cm^{-1}) (data not shown). Thus, these results suggest that the single, photolysis-sensitive γ-mode appears to be due to the histidylimidazole that is directly involved in the coordination of the heme moiety to the globin component, namely the proximal histidine.

MbO_2 Spectra and the Identification of the Liganded O_2 Stretching Frequency. FTIR spectra of liganded and photoproduct MbO_2 in the 1050–1150 cm^{-1} region are more complicated than those of MbCO due to the appearance of ν(O=O). Previous infrared[31] and resonance Raman[1,14,32] studies of oxymyoglobin have shown that the liganded O_2 mode is represented by several bands in the 1050–1150 cm^{-1} infrared region. Although the authors obtained similar data, there has been disagreement in the interpretations of these results. Caughey and co-workers[31] and Tsubaki and Yu[14] have attributed the multiple bands to coupling of ν(O=O) to an unidentified perturbation perhaps related to discrete conformational states. Kincaid and co-workers,[1,32] though not discounting the possibility of multiple states, have been able to use a single-conformer model to attribute the multiple O=O bands to coupling of the O=O modes to internal distal and/or proximal histidylimidazole modes.

A practical way of identifying the location of ν(O=O) is through photolysis, since the intensity of this band is expected to be reduced 40% in the cryogenic photoproduct and to increase as the ligand rebinds. This is a characteristic which would be absent in MbCO. Comparing the liganded and photoproduct second derivative spectra of MbO_2 to those of MbCO (Figure 3), ν(O=O) appears to fall at ~1105 cm^{-1}, overlapped by the proximal histidylimidazole γ-mode. The MbCO spectra clearly demonstrate that the unperturbed γ-band blue shifts by 2 cm^{-1} and increases in intensity upon photolysis. Quantitatively, the MbCO difference spectra (Figure 2A) show a 33% increase (from 0.0016 OD at 1105 cm^{-1} to 0.0024 OD at 1111 cm^{-1}) in the γ-band intensity upon photolysis. In MbO_2, however, the disappearance of Fe—O=O upon photolysis results in a *net decrease* in the γ-band intensity. Quantitatively, the MbCO difference spectra (Figure 2A) show a 33% increase (from 0.0016 OD at 1105 cm^{-1} to 0.0024 OD at 1111 cm^{-1}) in the γ-band intensity upon photolysis.

In MbO_2, however, the disappearance of Fe—O=O upon photolysis results in a *net decrease* in the γ-band intensity. Quantitatively, it decreases from 0.0015 OD at 1104 cm^{-1} to 0.0011 OD at 1111 cm^{-1} upon photolysis (Figure 2B). Potter et al.[31] have used IR difference spectra of isotopically labeled $Mb^{18}O_2$, $Mb^{17}O_2$, and $Mb^{16}O_2$ in order to "subtract out" any protein or solvent contributions and obtain absorption signatures exclusively due to ν(O=O). On the basis of their published data, we estimate the extinction coefficient for the O=O stretch to be ~0.22 OD cm^{-1} mM^{-1}. For the data presented here (4.3 mM and 0.0025 cm path length), one would expect to see an absorbance on the order of 0.0024 OD for the O=O contribution. Photolyzing 40% of the MbO_2 (photolysis quantum yield of MbO_2) would result in a decrease in optical density of 0.0009 OD at 1105 cm^{-1}. Therefore, subtracting the O=O contribution from the liganded γ-band intensity results in an absorbance of 0.0006 OD due to

the proximal histidylimidazole γ-mode. A 33% increase in the proximal histidylimidazole mode intensity upon photolysis would result in an absorbance of 0.0008 OD at 1111 cm^{-1}, which is on the same order of magnitude as the value obtained experimentally from the FTIR difference spectra presented here (0.0011 OD). Therefore, the contribution of ν(O=O) to the intensities of the liganded and photoproduct γ-modes is consistent with previous FTIR experiments done on oxymyoglobin.

In summary, the FTIR experiments we present support the theory of Kincaid and co-workers that ν(O=O) couples with a distal and/or proximal histidine mode. In contrast, however, we observe only a single, photolyzable Fe—O=O mode at 1105 cm^{-1}, overlapping the proximal histidylimidazole γ-mode at the same frequency. As is clear from the MbCO spectra, it is only a small component of the total γ-band intensity.

MbCO vs MbO_2 Spectra and the Electronic/Structural Nature of the Photolysis-Sensitive Protein and Heme Modes. Upon photolysis of a myoglobin ligand, a cascade of structural and electronic changes occur. The electron density on the iron increases. The spin state of the iron changes from low-spin to high-spin. High-spin hemes have longer iron–pyrrole bonds due to partially filled antibonding $d_{x^2-y^2}$ orbitals.[51] Five-coordinate, high-spin hemes, such as the MbCO photoproduct and deoxy Mb, relieve this repulsion by moving the iron atom out of the plane of heme, toward the proximal histidine. These out-of-plane heme structures display significant ruffling and doming of the porphyrin ring.[52] Subsequently, the proximal histidine leads a global movement of atoms on the proximal side of the heme plane, while the movement on the distal side involves local motions of several distal heme pocket R-groups, including the distal histidylimidazole.[53]

The structural and electronic changes that occur upon photolysis of a myoglobin ligand have a distinct effect on the infrared bands observed in the 1050–1150 cm^{-1} region. Table 1 shows results of the MbCO and MbO_2 liganded and photoproduct spectra.

A. Bandshifts. Numerous RR studies[24,51,54–57] have identified high frequency modes that are sensitive to changes in iron spin state, heme electron density, porphyrin core size, and heme peripheral substituents. The trends observed in core size, spin-state, and oxidation state markers can be used to explain the bandshifts of the α- and β-vinyl modes that we observe upon photolysis of MbCO and MbO_2.

Spin-state/core size markers involve the skeletal modes of the porphyrin ring structure.[55] Several high frequency Raman modes have been assigned as spin state markers to various low-spin and high-spin iron[56] porphyrins.[55] The general trend is a decrease in marker vibrational frequency as spin state changes from low- to high-spin. Porphyrin core expansion, due to steric and electronic effects of axial ligands, can affect the spin state marker frequencies.[51] Porphyrin doming and/or core expansion both result in a disruption in the π delocalization in the porphyrin ring, resulting in the decreased frequencies.[51,52,58]

Oxidation state markers have been assigned in fluoromet Hb (Fe^{III}) and deoxy Hb (Fe^{II}).[57] The observed trend is a decrease in frequency with an increase in electron density on the iron. It has been shown by X-ray absorption spectroscopy[59] that the iron electron density in various myoglobin cryogenic intermediate states increases in the following order: $MbCO_{liganded}$ < $MbCO_{photoproduct}$ < deoxy Mb. A greater iron electron density causes its d-orbitals to overlap the porphyrin π^* orbitals to a greater extent, resulting in an increased donation to the π^* orbitals on the porphyrin ring. In turn, the porphyrin ring bonds are weakened, reducing their vibrational frequencies.[57]

We have identified two heme peripheral vinyl modes (α and β) in liganded myoglobin that are red shifted to deoxy-like positions upon photolysis. These peripheral vinyl modes actively participate in the porphyrin π system. Therefore, just as the high-frequency oxidation state, core size, and spin state markers are red shifted with a disruption in the porphyrin π system, so are the two new structural markers that we have identified as peripheral vinyl modes. Because the α and β bands follow the same shifting pattern upon photolysis, i.e., 4 cm^{-1} red shifts, the shifts are more than likely due to the electronic changes that are known to occur in the porphyrin π system upon photolysis, rather than structural and/or electronic changes that occur between vinyl group and globin contacts.

The 1115 cm^{-1} photoproduct mode (ϵ band) has been assigned to a ring-vinyl stretch. This band has also been assigned as such in $Mb^{III}F$ and deoxy Mb by RR spectroscopy.[23] This band is an important structural marker, because it is unique to high-spin species where the iron atom is out of the heme plane, notably the myoglobin photoproduct,[59] deoxy Mb,[60] $Mb^{III}F$,[23] and $Fe^{III}PP$ IX.[61] The feature is completely absent in liganded MbCO, which is low-spin, and where the iron is completely in the heme plane. The band is sensitive to spin-state but not to oxidation state; this ring-vinyl stretch is present in the MbCO photoproduct (Fe^{II}, high-spin), $Mb^{III}F$ (Fe^{III}, high-spin), and $Fe^{III}PP$ IX (Fe^{III}, high-spin) and absent in liganded MbCO (Fe^{II}, low-spin). Since iron is slightly out of the heme plane in liganded MbO_2 and it has been proposed that MbO_2 has an intermediate spin state,[16,62] one sees a small 1115 cm^{-1} contribution (Figure 3).

The γ band has been assigned as a C–H bending mode of the proximal histidine. It is blue shifted upon photolysis. This shift could be attributed to any of the many structural and/or electronic changes that occur with the proximal histidine upon photolysis. For example, X-ray crystallographic data have revealed that, in deoxy Mb, the proximal histidine is tilted with respect to the heme plane, whereas it is perpendicular to the heme plane in liganded MbCO.[18,53,60] The tilt of the histidine, coupled with a decreased iron–histidine bond length, causes an increased heme–histidine repulsion in deoxy Mb. Numerous studies on the nature of the iron–proximal histidine bond[63–68] have interpreted this effect as resulting in a weakened Fe–His bond, decreasing the ν(Fe–His). Increased heme–histidine repulsion implies greater repulsion between the histidylimidazole hydrogens and the heme plane. This closeness may prohibit the histidine C–H bonds from bending freely, affecting the C–H bending mode frequency, i.e., causing a shift in the γ band upon photolysis.

B. Bandwidths. As can be seen by comparing the second derivative spectra of MbCO and MbO_2 (Figure 3), the α-, β-, and γ-bandwidths differ in MbCO versus MbO_2. This can partially be explained by understanding the nature of the photolysis quantum yield differences between MbCO and MbO_2. MbCO

(50) Tsuboi, M. In *Vibrational Spectroscopy—Modern Trends*; Barnes, A. J., Orville-Thomas, W. J., Eds.; Elsevier Publishing Co.: New York, 1977; p 405.
(51) Spiro, T. G.; Stong, J. D.; Stein, P. *J. Am. Chem. Soc.* **1979**, *101*, 2648.
(52) Hoard, J. L. *Science* **1971**, *174*, 1295.
(53) Kuriyan, J.; Wilz, S.; Karplus, M.; Petsko, G. A. *J. Mol. Biol.* **1986**, *192*, 133.
(54) Kitagawa, T.; Kyogoku, Y.; Iizuka, T.; Saito, M. I. *J. Am. Chem. Soc.* **1976**, *98*, 5169.
(55) Spiro, T. G.; Burke, J. M. *J. Am. Chem. Soc.* **1976**, *98*, 5482.
(56) Rimai, L.; Salmeen, I.; Petering, D. H. *Biochemistry* **1975**, *14*, 378.
(57) Spiro, T. G.; Strekas, T. C. *J. Am. Chem. Soc.* **1974**, *96*, 340.
(58) Spaulding, L. D.; Chang, C. C.; Yu, N. T.; Felton, R. H. *J. Am. Chem. Soc.* **1975**, *97*, 2517.
(59) Chance, B.; Fischetti, R.; Powers, L. *Biochemistry* **1983**, *22*, 3820.
(60) Takano, T. *J. Mol. Biol.* **1977**, *110*, 569.
(61) Radonovich, L. J.; Bloom, A.; Hoard, J. L. *J. Am. Chem. Soc.* **1972**, *94*, 2073.
(62) Petrich, J.; Poyart, C.; Martin, J. *Biochemistry* **1988**, *27*, 4049.
(63) Gelin, B. R.; Karplus, M. *Proc. Natl. Acad. Sci. U.S.A.* **1977**, *74*, 801.
(64) Warshel, A. *Proc. Natl. Acad. Sci. U.S.A.* **1977**, *74*, 1789.
(65) Olafson, B. D.; Goddard III, W. A. *Proc. Natl. Acad. Sci. U.S.A.* **1979**, *74*, 1315.
(66) Friedman, J. M.; Rousseau, D. L.; Ondrias, M. R.; Stepnoski, R. A. *Science* **1982**, *218*, 1244.
(67) Gelin, B. R.; Lee, A. W. M.; Karplus, M. *J. Mol. Biol.* **1983**, *171*, 489.
(68) Friedman, J. M.; Scott, T. W.; Fisanick, G. J.; Simon, S. R.; Findsen, E. W.; Ondrias, M. R.; MacDonald, V. W. *Science* **1985**, *229*, 187.

Table 2. Full-Width, Half-Maximum Bandwidths (in cm^{-1}) of Photolysis-Sensitive Bands in the Second Derivative Myoglobin FTIR Spectra

	α	β	γ	ϵ
$MbCO_{liganded}$	3	4	6	
$MbCO_{photoproduct}$	3	4	4	3
$Mb^{16}O_{2liganded}$	5	4	7	
$Mb^{16}O_{2photoproduct}$	6	5	9	
deoxy Mb	3	3	4	3

has a narrow distribution of substates (with respect to the peripheral vinyl group environments) in the case of liganded α and β bands (narrow bandwidths.) A photolysis quantum yield of 1.0 for MbCO indicates that the MbCO bound states are entirely converted to stable photoproduct, in this case resulting in narrow α- and β-photoproduct bands, similar to those of deoxy Mb (Table 2). The wider bandwidth of the liganded γ-mode (6 cm^{-1}) indicates multiple environments for this mode (proximal histidine), the blue edge of which has an environment that resembles the histidine environment in the photoproduct. Photolysis results in a more homogeneous environment, resulting in a narrower bandwidth of the γ-photoproduct band. These data suggest multiple substates in the liganded MbCO histidine mode but not in the photoproduct.

In MbO_2, the liganded α and γ bands have wider bandwidths (Table 2), indicating a wider distribution of peripheral vinyl group and proximal histidine environments. In the case of the γ-mode, the presence of ν(O=O) may also contribute to the width of that band. Photolysis of MbO_2 produces a maximum 40% stable photoproduct,[16] resulting in photoproduct distributions that contain substantial liganded material. The increased widths of the MbO_2 liganded and photoproduct spectra cause them to overlap more than those of MbCO. This overlap region can be attributed to the 60% of the MbO_2 molecules that are seemingly unphotolyzable. More specifically, the distribution of vinyl environments at the *red* edge (lower frequency) of the liganded α and β bands does not photolyze, whereas those at the blue edge do. In the case of the γ-liganded band, it is the *blue* edge of the histidine distribution that does not photolyze.

Conclusion

Low-temperature FTIR experiments of liganded and photoproduct MbCO and MbO_2 have revealed significant differences in the liganded and photoproduct infrared spectra between 1050 and 1150 cm^{-1}. For MbCO, we observe liganded modes at 1080 and 1096 cm^{-1} that shift to 1076 and 1092 cm^{-1}, respectively, upon photolysis. Model compound studies on Fe^{III}OEP and Fe^{III}-PP IX have aided in assignment of these modes to the heme peripheral vinyl groups, which are structurally and/or electronically affected by photolysis. A third MbCO liganded mode at 1107 cm^{-1} is assigned to a C–H bending mode of the proximal histidine. It shifts to 1109 cm^{-1} upon photolysis due to environmental changes in the proximal histidine. This result can be compared with earlier studies[27,28] that have identified similar histidine–heme complex modes that are redox-sensitive. Finally, we identify a band at 1115 cm^{-1} that is unique to the MbCO photoproduct and is only observed in heme compounds in which the iron is out of the heme plane.

For MbO_2, the liganded α- and β-vinyl modes are red shifted from 1080 and 1096 cm^{-1} to 1076 and 1094 cm^{-1}, respectively, and the liganded γ-mode is blue shifted from 1105 to 1107 cm^{-1} upon photolysis. These bands shift incompletely in MbO_2 when compared to MbCO, which is related to the photolysis quantum yield difference between the two ligands and not necessarily to differences in the photoproduct intermediates. The MbO_2 spectrum between 1050 and 1150 cm^{-1} also contains a contribution from the dioxygen stretching frequency. We observe a single photolyzable Fe—O=O mode at 1105 cm^{-1}, overlapped by a proximal histidine C–H bending mode at the same frequency. The intensity of ν(O=O) is small with respect to the overall intensity of the proximal histidine γ-mode.

These results provide direct structural markers for liganded and photoproduct states of myoglobin, which are imperative in understanding the intermediate states involved in ligand binding. On a larger scale, the technique of using FTIR at cryogenic temperatures can be used in the same fashion on many biological systems for trapping and characterizing intermediate states involved in a myriad of light-initiated biochemical reactions.

Acknowledgment. We gratefully thank the reviewers for their helpful comments and the National Institutes of Health for support of this work (HL45892).